AGU PUBLICATIONS

Geophysical Research Letters

RESEARCH LETTER
10.1002/2016GL071569

Key Points:
- Models of earthquake nucleation have been developed using SAFOD data and measurements of friction properties of drill core samples
- The nucleation process of *M* 2 repeaters near the SAFOD observatory may consist of two distinct phases, like in that of laboratory earthquakes
- Our results indicate that the precursory signals of anticipated *M* 2 earthquakes could be captured by near-field strain observations

Supporting Information:
- Supporting Information S1

Correspondence to:
Y. Kaneko,
y.kaneko@gns.cri.nz

Citation:
Kaneko, Y., B. M. Carpenter, and S. B. Nielsen (2016), Nucleation process of magnitude 2 repeating earthquakes on the San Andreas Fault predicted by rate-and-state fault models with SAFOD drill core data, *Geophys. Res. Lett.*, *44*, doi:10.1002/2016GL071569.

Received 11 OCT 2016
Accepted 28 DEC 2016
Accepted article online 30 DEC 2016

Nucleation process of magnitude 2 repeating earthquakes on the San Andreas Fault predicted by rate-and-state fault models with SAFOD drill core data

Yoshihiro Kaneko[1], Brett M. Carpenter[2,3], and Stefan B. Nielsen[4]

[1]GNS Science, Lower Hutt, New Zealand, [2]School of Geology and Geophysics, University of Oklahoma, Norman, Oklahoma, USA, [3]Istituto Nazionale di Geofisica e Vulcanologia, Rome, Italy, [4]Department of Earth Sciences, University of Durham, Durham, UK

Abstract Recent laboratory shear-slip experiments conducted on a nominally flat frictional interface reported the intriguing details of a two-phase nucleation of stick-slip motion that precedes the dynamic rupture propagation. This behavior was subsequently reproduced by a physics-based model incorporating laboratory-derived rate-and-state friction laws. However, applying the laboratory and theoretical results to the nucleation of crustal earthquakes remains challenging due to poorly constrained physical and friction properties of fault zone rocks at seismogenic depths. Here we apply the same physics-based model to simulate the nucleation process of crustal earthquakes using unique data acquired during the San Andreas Fault Observatory at Depth (SAFOD) experiment and new and existing measurements of friction properties of SAFOD drill core samples. Using this well-constrained model, we predict what the nucleation phase will look like for magnitude ~2 repeating earthquakes on segments of the San Andreas Fault at a 2.8 km depth. We find that despite up to 3 orders of magnitude difference in the physical and friction parameters and stress conditions, the behavior of the modeled nucleation is qualitatively similar to that of laboratory earthquakes, with the nucleation consisting of two distinct phases. Our results further suggest that precursory slow slip associated with the earthquake nucleation phase may be observable in the hours before the occurrence of the magnitude ~2 earthquakes by strain measurements close (a few hundred meters) to the hypocenter, in a position reached by the existing borehole.

1. Introduction

Earthquake rupture initiates within a limited nucleation patch then accelerates and propagates over the fault area, at a speed close to the shear wave velocity of the surrounding rocks (a few km/s). A question of critical importance is whether earthquake rupture begins abruptly or starts to grow slowly and which set of parameters determine one or the other condition. Indeed, a slow, aseismic slip front (representing the moving boundary between slipping and stuck regions on the fault surface) may expand in the nucleation region for extended time intervals before the breakout of seismic rupture. The controls on the size and duration of such an aseismic phase are of extreme interest in seismology.

While most earthquake ruptures start abruptly, with no evidence for a nucleation process, precursory aseismic slip prior to the initiation of many well-studied earthquakes has been inferred from seismological observations. Studies of well-recorded seismicity in various tectonic settings provide observational evidence that precursory aseismic slip triggers the failure of small-scale asperities, generating foreshocks near the eventual hypocenter of the main shock [*Dodge et al.*, 1996; *McGuire et al.*, 2005; *Bouchon et al.*, 2011; *Tape et al.*, 2013; *Schurr et al.*, 2014; *Yabe et al.*, 2015]. It was pointed out [*Bouchon et al.*, 2013] that foreshock activity is preferentially observed in interplate, as opposed to intraplate faulting. In the case of the 2004 *M* 9.2 Sumatra-Andaman earthquake, subsidence within the 6–12 months was interpreted as precursory slow slip of up to 1.5 m preceding the seismic rupture [*Paul and Rajendran*, 2015]. In the case of the 2011 *M* 9.0 Tohoku-oki earthquake, *Kato et al.* [2012] reported that foreshock sequences migrated toward the hypocenter at a speed of 2–5 km/d over a period of a few weeks, followed by a pause of about 10 days, and then again at a slightly higher (~10 km/d) speed in the hours preceding the earthquake, suggesting transient propagation of a slow-slip rupture front. However, direct observations of precursory aseismic slip remain a major challenge, likely due to the paucity of in situ monitoring at seismogenic depths. An additional difficulty is our incomplete understanding of the

length scale and timescale of the nucleation process and its dependence on rock type, tectonic stress, and stressing rate.

Accumulating evidence from laboratory and theoretical studies suggests that an aseismic nucleation precedes rapid shear-slip events on a frictional interface. In laboratory studies, the nucleation process of shear ruptures on a frictional interface is often characterized by a transition from slow (quasi-static) to fast (inertially controlled) rupture, which can be qualitatively understood as the onset of a stick-slip frictional instability [e.g., *Ohnaka and Kuwahara*, 1990; *Kato et al.*, 1992; *Ohnaka*, 1996; *Dieterich and Kilgore*, 1996; *Nielsen et al.*, 2010; *Latour et al.*, 2013; *McLaskey and Kilgore*, 2013]. Theoretical and numerical studies support the view that earthquake nucleation is a developing frictional instability on a fault under tectonic loading [e.g., *Okubo and Dieterich*, 1984; *Dieterich*, 1992; *Tullis*, 1996; *Campillo and Ionescu*, 1997; *Shibazaki and Matsu'ura*, 1998; *Lapusta and Rice*, 2003; *Hori et al.*, 2004; *Ampuero and Rubin*, 2008; *Kaneko and Lapusta*, 2008; *Fang et al.*, 2010; *Schmitt et al.*, 2011; *Kaneko and Ampuero*, 2011; *Noda et al.*, 2013; *Viesca*, 2016].

In particular, theoretical models of earthquake nucleation based on rate-and-state friction laws were developed by a number of investigators [e.g., *Okubo and Dieterich*, 1984; *Dieterich*, 1992; *Tullis*, 1996; *Lapusta and Rice*, 2003; *Hori et al.*, 2004; *Ampuero and Rubin*, 2008; *Kaneko and Lapusta*, 2008; *Fang et al.*, 2010; *Kaneko and Ampuero*, 2011; *Noda et al.*, 2013; *Viesca*, 2016]. However, the validation of these models with observed nucleation, even in idealized laboratory analogue experiments, is a challenging task because the resulting nucleation behavior is highly nonlinear and depends on the underlying assumptions in each model. Recently, *Kaneko et al.* [2016] demonstrated that the relatively simple model of rupture nucleation with rate-and-state friction quantitatively reproduces the spatial and temporal evolution of nucleating ruptures observed in high-resolution laboratory experiments over a range of normal stresses [*Latour et al.*, 2013], validating the rate-and-state model at a laboratory scale (i.e., tens of centimeters). Yet it is not clear whether the laboratory-scale model can be applied to the nucleation of crustal earthquakes for two main reasons. First, scaling up the laboratory results to crustal conditions requires orders of magnitude changes in the fault size, normal stress, and background loading rate. Second, and more importantly, the physical and friction properties of fault zone rocks at seismogenic depths are generally unknown.

In this study, we conduct numerical simulations of earthquake nucleation using the model proposed by *Kaneko et al.* [2016] which was validated with laboratory results [*Latour et al.*, 2013]. We adapt and parametrize the numerical model according to data acquired during the SAFOD experiment and new and existing measurements of friction properties of SAFOD drill core samples. We then predict what the nucleation phase will look like for magnitude (M) ~2 repeating earthquakes at a 2.8 km depth and examine whether such phase can be observable prior to the onset of earthquake rupture. Lastly, implications of our results for the nucleation of other crustal earthquakes are discussed.

2. Model Setup

A two-dimensional elastodynamic model [*Liu and Lapusta*, 2008; *Lapusta and Liu*, 2009] is used to simulate the nucleation of in-plane shear-slip events on a fault embedded into an infinite elastic medium and subject to slow tectonic loading. In this model, fast shear-slip events (i.e., earthquakes) are generated as a part of spontaneous earthquake sequences, with conditions before the nucleation naturally arising from the previous history of fault slip and loading. The numerical approach is based on a boundary-integral method, and its implementation is described in *Liu and Lapusta* [2008] and *Lapusta and Liu* [2009].

The fault constitutive response is governed by laboratory-derived rate-and-state friction laws [*Dieterich*, 1979; *Ruina*, 1983]. Frictional resistance τ of the fault may be shown as

$$\tau = (\sigma - p)\left[f_0 + a\ln\left(\frac{V}{V_0}\right) + b\ln\left(\frac{V_0\theta}{D_c}\right)\right] \tag{1}$$

$$\frac{d\theta}{dt} = -\left(\frac{V\theta}{D_c}\right)\ln\left(\frac{V\theta}{D_c}\right) \tag{2}$$

where σ is the normal stress, p is the pore pressure on the fault, $\sigma - p$ is the effective normal stress, a and b are constitutive parameters, V is slip rate, f_0 is the reference friction coefficient associated with the reference slip rate V_0, D_c is the characteristic slip distance, and θ is a state variable often interpreted as the average age

of the population of contacts between two surfaces [*Dieterich*, 1979; *Ruina*, 1983]. In this study, the so-called "slip law" is assumed for the evolution of the state variable (equation (2)). Compared to the widely used aging law [*Dieterich*, 1979; *Ruina*, 1983], the slip law provides a better match to velocity-step rock-friction experiments [*Rathbun and Marone*, 2013; *Bhattacharya et al.*, 2015] and hence would be more appropriate for modeling earthquake nucleation. Note that the slip law fails to quantitatively explain fault healing processes in laboratory experiments [*Beeler et al.*, 1994] and would not be appropriate for simulating postseismic and interseismic slip. Which state-variable evolution law is the most appropriate for modeling overall properties of the earthquake cycle is still under debate [e.g., *Beeler et al.*, 1994; *Bhattacharya et al.*, 2015; *Marone and Saffer*, 2015].

In the rate-and-state framework, whether the fault patch deforms as a stick-slip event or continuous creep depends on the friction parameter $a-b$. At steady state, rock friction shows either rate-weakening ($a-b<0$) or rate strengthening ($a-b>0$) behavior, influenced by a number of factors including temperature, normal stress, and the type of materials [e.g., *Blanpied et al.*, 1998; *Ikari et al.*, 2011a; *Collettini et al.*, 2011; *Mitchell et al.*, 2016]. A stick-slip frictional instability is able to develop only if the rate-weakening patch of a fault exceeds the nucleation length h^*. The estimate of a critical length h^* appropriate for the friction laws (equations (1) and (2)) was theoretically derived from the linear stability analysis of steady sliding between deformable solids [*Rice*, 1993; *Ruina*, 1983]:

$$h^*_{\mathrm{RR}} = \frac{\pi}{4}\frac{\mu' D_c}{(\sigma - p)(b-a)}\ , \tag{3}$$

where $\mu' = \mu/(1-\nu)$ and $\mu' = \mu$ are for in-plane and antiplane sliding, respectively, μ is the shear modulus, and ν is the Poisson's ratio.

3. Main Results From the Study of *Kaneko et al.* [2016]

We summarize here the main results of laboratory-scale simulations already discussed in *Kaneko et al.* [2016] to facilitate comparisons with the nucleation simulations of SAFOD earthquakes considered in this study.

The model setup considered in *Kaneko et al.* [2016] was motivated by the laboratory finding of *Latour et al.* [2013]. In the laboratory analogue experiments, spontaneous rupture nucleation on a frictional interface was imaged and captured via high-speed photoelasticity and acoustic sensors (Figure 1a). In the numerical models, the fault is divided into three segments: a central rate-weakening patch and the surrounding rate-strengthening segments that mimic thin coating of viscous silicon patches in the laboratory experiments (Figure 1b). A background time-independent stressing rate $\dot{\tau}$ is uniformly applied along the fault and acts as loading. At both ends of the fault, zero-displacement boundary conditions are imposed for simplicity. The consequences of these model assumptions on the resulting nucleation are discussed in *Kaneko et al.* [2016]. Physical and numerical parameters are shown in Table 1 and described in Text S1 in the supporting information.

Using this relatively simple fault model with the parameters derived from the laboratory experiments of *Latour et al.* [2013], *Kaneko et al.* [2016] reproduced the detailed characteristics of observed shear rupture nucleation: (i) The positions of simulated rupture fronts under different effective normal stresses $\bar{\sigma}$ agree well with those in the laboratory experiments (Figures 1c–1e). (ii) For a range of $\bar{\sigma}$, the nucleation is composed of two distinct phases: slow, quasi-static propagation phase (first low slope) and faster acceleration phase (high slope), both of which are likely aseismic processes, followed by dynamic rupture propagation phase (Figures 1f and 1g). (iii) The length at which the rupture transitions from the quasi-static to acceleration phase can be approximately predicted by a theoretical estimate of critical nucleation length h^*_{RR} (equation (3)) (Figure 1f). (iv) However, the transition length is also affected by the background loading rate to some extent. (v) The growth of rupture for a range of $\bar{\sigma}$ appears to be controlled by the critical nucleation length and breakdown power density.

4. SAFOD Data

We apply our model of rupture nucleation described above to unique data acquired by the San Andreas Fault Observatory at Depth (SAFOD) geophysical experiment [*Zoback et al.*, 2011]. Near the SAFOD borehole which penetrated three active strands of the San Andreas Fault at ~2.7 km depth including the southwest deforming zone (SDZ) and the central deforming zone (CDZ), three clusters of $M \sim 2$ repeating earthquakes were previously identified (Figure 2). These seismic events recur every few years at the same location and generate

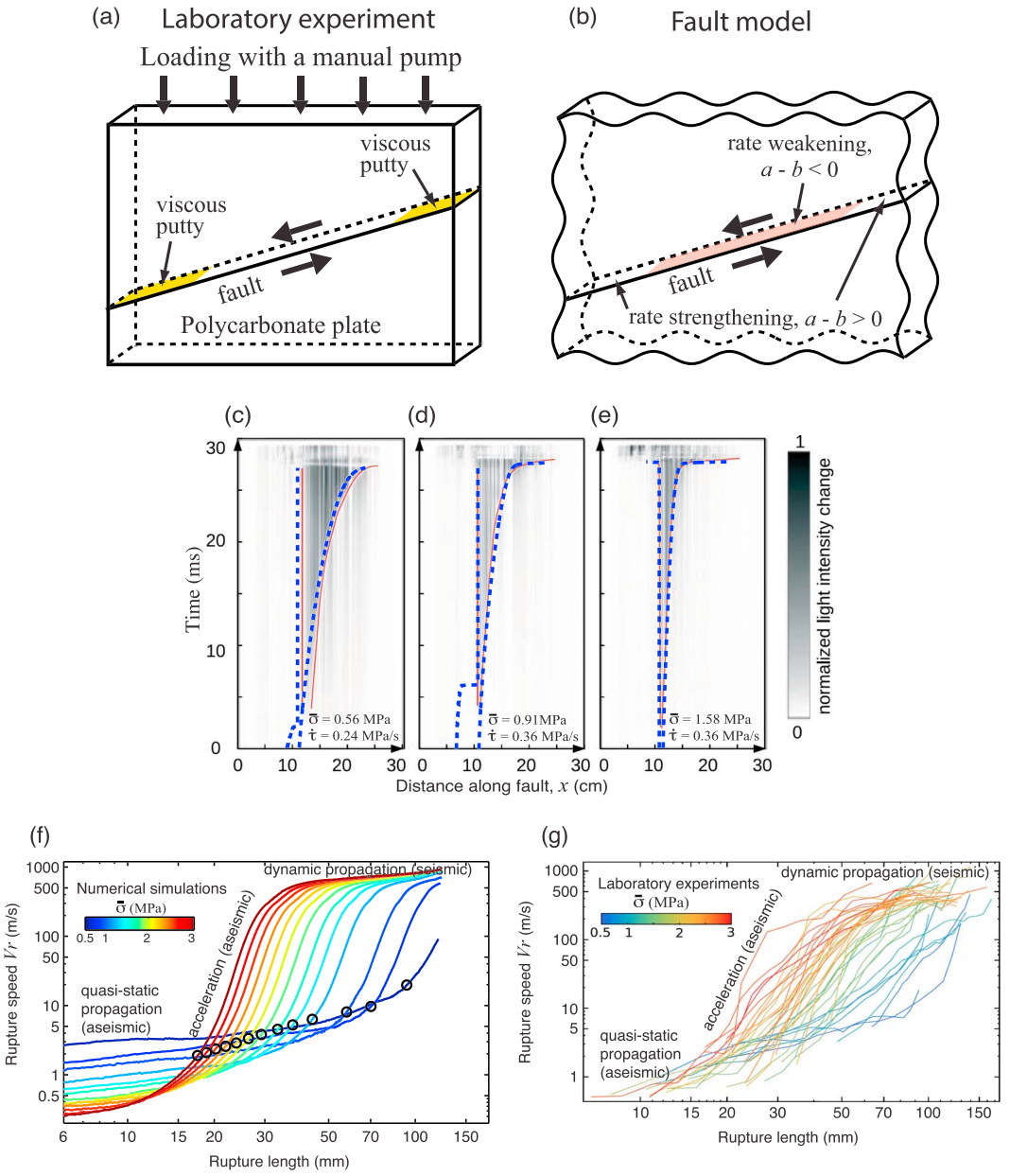

Figure 1. Schematic diagrams illustrating the setup of (a) the laboratory experiments of *Latour et al.* [2013] and (b) the model of *Kaneko et al.* [2016]. (c–e) Positions of rupture fronts during a transition from quasi-static to dynamic rupture in numerical simulations with different normal stresses σ (dashed blue), which are superimposed on the positions of observed rupture tips in laboratory experiments (red), with a gray scale showing the light intensity change indicating the actively slipping zone. The rupture fronts are defined as the locations of two peak shear stresses: one within the left rate-strengthening patch and the other within the rate-weakening patch. (f and g) Characteristics of nucleation phase under a different effective normal stress $\bar{\sigma}$ in numerical simulations and for 47 stick-slip events in laboratory experiments. The rupture length (horizontal axis) is defined as a distance from the left edge of the rate-weakening patch to the rupture front. Open circles correspond to theoretical estimates of nucleation length h^*_{RR}. Observed and modeled rupture speeds increase with the rupture length. The evolution of the rupture front under a range of $\bar{\sigma}$ closely matches the laboratory results.

Table 1. Estimated Nucleation Size h^*_{RR} From the SAFOD Geophysical Logs and Laboratory Friction Experiments [*Carpenter et al.*, 2015][a]

	Wall Rock Near the SDZ	Serpentine in the SDZ	Wall Rock Near the CDZ	Polycarbonate (Laboratory)
Depth (m)	3190.57	3192.87	3303.57	NA
P wave speed V_p (m/s)	4963	2973	3722	1860
S wave speed V_s (m/s)	2986	1743	2069	893
Density ρ (kg m^{-3})	2613	2478	2372	1200
Shear modulus μ (GPa)	23.3	7.53	10.15	0.96
Poisson's ratio ν	0.216	0.238	0.277	0.35
Effective stress $(\sigma - p)$ (MPa)	122	122	122	0.56–3.0
Rate and state parameter a	0.00661	0.00338	0.00951	0.0100
Rate and state parameter b	0.00894	0.00374	0.01081	0.0144
$b - a$	0.00233	0.00036	0.00130	0.0044
a/b	0.739	0.904	0.880	0.694
Characteristic slip D_c (μm)	233	239	221	0.2
Nucleation size h^*_{RR} (m)	19	42	15	$17–93 \times 10^{-3}$

[a]Depth corresponds to measured depth along the Phase 2 SAFOD borehole [*Zoback et al.*, 2011]. The SAFOD borehole passes through the southwest deforming zone (SDZ) and the central deforming zone (CDZ). Frictional properties of cuttings and core samples recovered from the SAFOD borehole were measured in laboratory experiments at 25 MPa effective normal stress under saturated and confined conditions [*Carpenter et al.*, 2015]. Shear modulus and Poisson's ratio are calculated from V_p, V_s, and density. Parameters used in the study of laboratory-scale nucleation [*Kaneko et al.*, 2016] are also shown.

similar seismic signals. Among them, the "Hawaii" cluster of repeating earthquakes is located ~100 m below the drill hole, apparently near or within the 2 m wide SDZ (Figure 2). Repeating earthquakes are believed to rupture a rate-weakening patch surrounded by a creeping region [e.g., *Beeler et al.*, 2001; *Chen and Lapusta*, 2009; *Chen et al.*, 2010]; accordingly, we may use the modeling approach described in section 2, combined with SAFOD data, to simulate the nucleation process.

Existing measurements of friction properties of cuttings and core samples recovered at the depths of ~2.7 km show that materials within the SDZ and CDZ generally exhibit steady state rate-strengthening frictional behavior favoring aseismic sliding and consistent with the creeping segment of the San Andreas Fault. Rate-weakening frictional behavior is also reported for wall rocks near the SDZ and CDZ as well as serpentine in the SDZ [*Carpenter et al.*, 2012, 2015; *Moore et al.*, 2016]. The wall rocks near the SDZ consist of sheared siltstones and shales, whereas the wall rocks near the CDZ consist of sheared siltstones, mudstones, and sandstones. The serpentine within the SDZ is mostly lizardite with some chrysotile [*Moore and Rymer*, 2012; *Carpenter et al.*, 2015]. Since repeating earthquakes are thought to nucleate within rate-weakening fault patches surrounded by a creeping (rate-strengthening) region, we assume that they occur in rocks that are identical to the SAFOD core samples with rate-weakening frictional behavior.

In situ physical properties obtained from the SAFOD geophysical log data [*Zoback et al.*, 2011] and measurements of friction properties of recovered core samples [*Carpenter et al.*, 2015] provide constraints on most model parameters. The physical properties of relevant rocks at the SAFOD depths are shown in Table 1. Shear modulus and Poisson's ratio are calculated from the measurements of compressional and shear wave speeds and density. On the basis of stress measurements from the SAFOD pilot hole, an estimate of the effective normal stress on the fault at the SAFOD depth is 122 MPa [*Hickman and Zoback*, 2004]. Since the existing measurements of friction parameters [*Carpenter et al.*, 2015] are based on a different form of rate-and-state friction laws, we measure friction parameters a, b, and D_c by fitting the assumed friction laws (equations (1) and (2)) to the laboratory data shown in Figures 3a–3c. Note that rate-and-state parameters a, b, and D_c on natural faults might be different from those measured in laboratory experiments as, for example, D_c depends on the gouge-zone thickness. We use laboratory-derived parameters because a narrow principal slip surface is generally required for velocity-weakening frictional behavior and hence the nucleation of an earthquake [e.g., *Ikari et al.*, 2011b] and because the rock samples are from the same materials present in the vicinity of the repeating earthquakes.

We find that wall rocks near the SDZ and CDZ show clear rate-weakening behavior, whereas serpentine in the SDZ is only slightly rate weakening, with $b - a = 0.00036$ (Figures 3a–3c). The estimated friction parameters

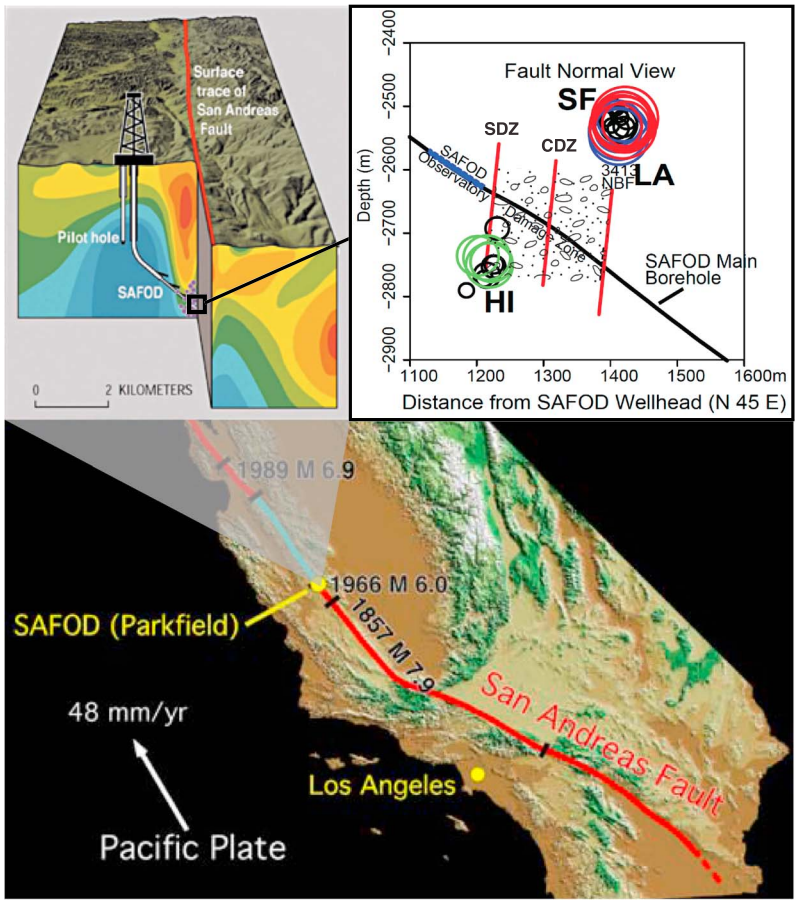

Figure 2. Locations of $M \sim 2$ repeating earthquakes (shown by colored circles) observed at the SAFOD depths [*Hickman et al.*, 2004; *Zoback et al.*, 2011]. Solid red lines show inferred extension of three deforming zones. The Hawaii (HI) cluster denoted by green circles targeted by a future SAFOD project is located ~100 m below the southwest deforming zone (SDZ) and 100–150 m away from the SAFOD observatory.

are broadly consistent with those of serpentinites and wall rock at equivalent stress conditions in other studies [*Reinen et al.*, 1991; *Moore et al.*, 2016]. The corresponding theoretical estimates of critical nucleation length h^*_{RR} for these core samples at SAFOD depths are in the range of 15–42 m (Figures 3d and 3e).

With these physical and friction parameters and stress conditions, we simulate the nucleation process of $M \sim 2$ repeating earthquakes on a fault consisting of a 100 m long central rate-weakening patch surrounded by rate-strengthening segments (Figure S1). Almost all the model parameters in the central rate-weakening patch are constrained by SAFOD data and the measurements of friction properties of (i) wall rock near the SDZ, (ii) serpentine in the SDZ, and (iii) wall rock near the CDZ. The model parameters in the rate-strengthening segments are the same as those in the rate-weakening patch except for b (Figure S1); the transition from the rate-weakening ($a - b < 0$) to rate-strengthening ($a - b > 0$) behavior can be attributed to changes in the fault rock type/composition or surface properties due to temperature and fluid content [*Moore and Rymer*, 2012; *Carpenter et al.*, 2015; *Moore et al.*, 2016]. The background loading rate $\dot{\tau}$ is chosen such that the recurrence interval T of repeating earthquakes is a few years (Figure S1), consistent with that of $M \sim 2$ repeating earthquakes at the SAFOD depth [*Zoback et al.*, 2011]. Since $\dot{\tau} = \Delta\tau/T$, assumed values of $\dot{\tau}$ imply that the stress drop $\Delta\tau \approx 1-2$ MPa, consistent with a typical value of stress drop for crustal earthquakes [e.g., *Kanamori and Anderson*, 1975] and from laboratory experiments on SAFOD materials [*Carpenter et al.*, 2012].

5. Simulated Nucleation of $M \sim 2$ Repeating Earthquakes

Despite up to 3 orders of magnitude difference in the physical and friction parameters and stress conditions, the behavior of the modeled nucleation of the Hawaii repeating earthquakes for materials with the properties of the wall rock near the SDZ and CDZ qualitatively resembles that of the laboratory earthquakes. A stress

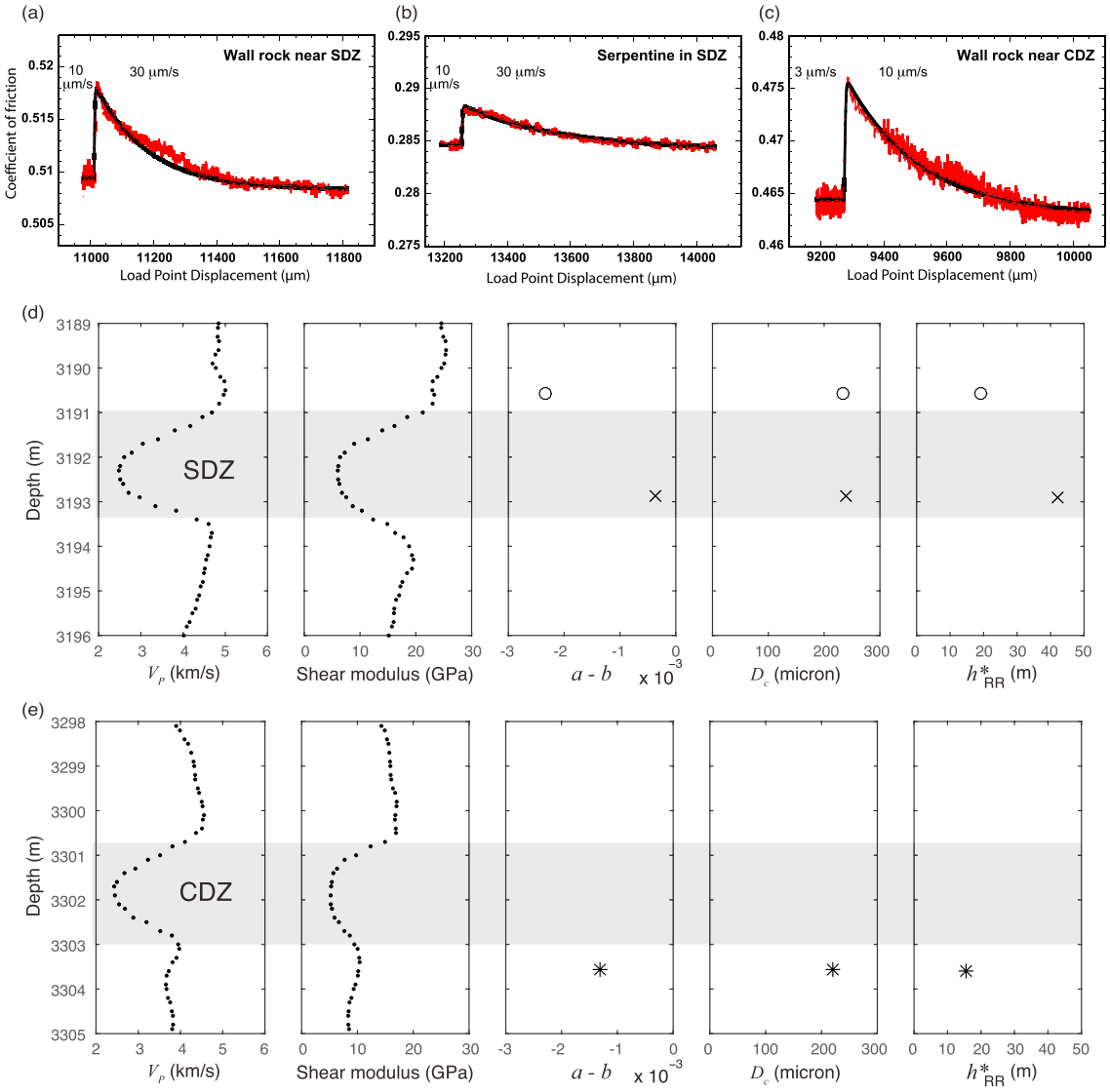

Figure 3. Fits to laboratory velocity-step experiments at 25 MPa effective normal stress. Raw data and modeling results for (a) an intact wafer of wall rock near the SDZ, (b) powdered serpentine from within the SDZ, and (c) an intact wafer of wall rock near the CDZ. Sliding velocities before and after the velocity step are indicated. The values of friction parameters are determined by fitting the laboratory data [*Carpenter et al.*, 2015] using an inverse modeling technique [*Blanpied et al.*, 1998] with the slip law state-variable evolution (equation (2)). The details of rate-and-state parameters are given in Table 1. (d and e) Measured friction parameters $a - b$, D_c, and the corresponding nucleation size h^*_{RR} for the SAFOD samples with rate-weakening behavior. Depth corresponds to measured depth along the Phase 2 SAFOD borehole. Measured *P* wave velocity and shear modulus from geophysical logs [*Zoback et al.*, 2011] are shown for reference. The SAFOD borehole passes through the southwest deforming zone (SDZ) and the central deforming zone (CDZ).

concentration (i.e., the rupture front) migrates inward from the edge of a rate-weakening patch, and the corresponding peak slip rate monotonically increases during nucleation (Figures 4a and 4c). Like in laboratory-scale nucleations, the propagation speed of the nucleating rupture front also increases monotonically (Figure 4g). Three phases of rupture evolution can be identified: an initial slow propagation phase characterized by the first low slope, faster acceleration phase (high slope), and rapid dynamic rupture propagation phase (final low slope) (Figure 4g). At the onset of the dynamic propagation phase, the rupture becomes bilateral and propagates through the entire rate-weakening patch and parts of the surrounding rate-strengthening segments (Figures 4d and 4f).

On the contrary, the case with serpentine in the SDZ shows a complex nucleation behavior. The main rupture front initially migrates in one direction and then propagates back in the opposite direction before it evolves into bilateral dynamic rupture (Figures 4b and 4e). The amount of slow slip associated with the

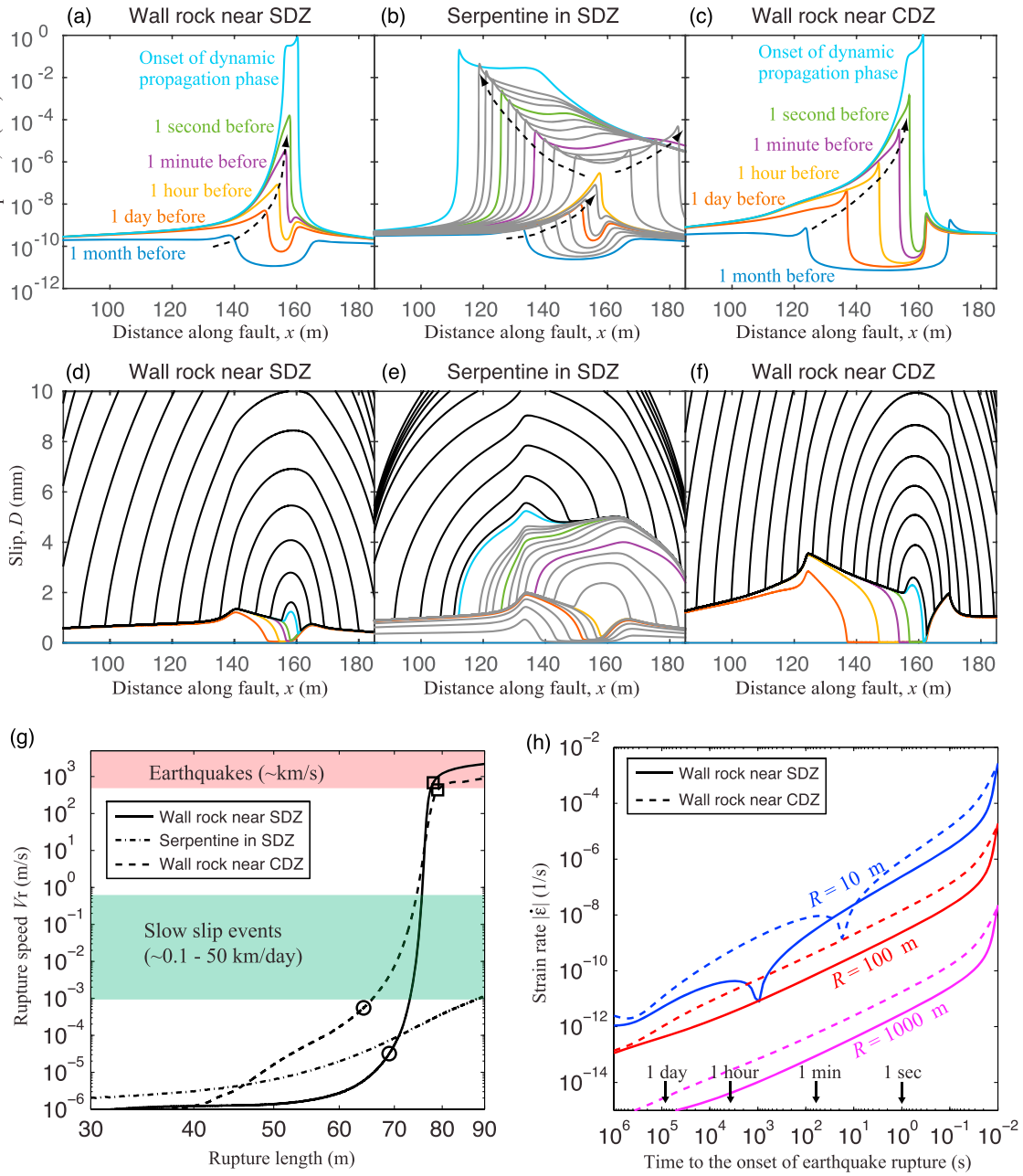

Figure 4. Simulated nucleation processes of repeating earthquakes near the San Andreas Fault Observatory at Depth (SAFOD) borehole. Snapshots of (a–c) slip rate and (d-f) slip distributions for materials with the properties of wall rocks near the southwest deforming zone (SDZ), serpentine in SDZ, and wall rocks near the central deforming zone (CDZ). Black contours show slip accumulation during the dynamic rupture propagation. For serpentine in SDZ, gray contours are added to show additional detail of slip accumulation during the nucleation. Arrows indicate the propagation direction of rupture front. (g) Rupture propagation speed versus rupture length. Rupture transitions from the quasi-static to acceleration phase (open circle) and from the acceleration to dynamic propagation phase (open square) are graphically determined from the intersections of adjacent linear segments. Rupture propagation speeds of earthquakes and slow slip events around the Pacific [*Gao et al.*, 2012] are also indicated for reference. (h) The magnitude of shear-strain rate versus time at different off-fault distances R from the eventual hypocenter.

nucleation process is also greater than the other cases (Figure 4e). This complex nucleation process results from the critical nucleation length being comparable to the size of the rate-weakening patch [e.g., *Rubin*, 2008; *Wei et al.*, 2013].

While the general behavior of SAFOD earthquake nucleation is qualitatively similar to laboratory-scale nucleations, the length scale and timescale are orders of magnitude different. For materials with the properties of the wall rock near the SDZ and CDZ, the resulting nucleation length, defined here by a rupture length at the

transition from the quasi-static to acceleration phase, is 3 orders of magnitude larger than the laboratory-scale counterpart (compare Figures 1f and 4g). Since shear modulus and D_c are much larger for the SAFOD samples than polycarbonate (see Table 1), the theoretical estimate of a critical nucleation length h^*_{RR} (equation (3)) is much larger. In addition, the modeled nucleation lengths are ~4 times larger than those predicted by h^*_{RR}. Slower loading generally results in a larger nucleation length as reported in laboratory studies [*Kato et al.*, 1992; *Ohnaka*, 1996] and numerical modeling [*Kato and Hirasawa*, 1996; *Kaneko et al.*, 2016].

For materials with the properties of the wall rock near the SDZ and CDZ, the acceleration phase begins at ~1 day before the onset of the dynamic propagation phase (Figure 4g). In the laboratory-scale simulations, the same phase starts at ~1 ms before the onset of the dynamic propagation phase (Figures 1c–1e). The orders of magnitude difference in the timescales is due to differences in the friction properties of the SAFOD samples and polycarbonate (Table 1) as well as in the background loading rates between the tectonic ($\dot{\tau} \approx 1$ MPa/yr) and laboratory ($\dot{\tau} \approx 0.4$ MPa/s) conditions. As discussed in *Kaneko et al.* [2016], the acceleration phase appears in an equivalent quasi-static simulation (i.e., without the inertial effect), suggesting that this phase is an aseismic process. In addition, moment rate acceleration starts to increase abruptly only from the onset of dynamic rupture propagation (Figure S2). Far-field velocity seismograms are proportional to moment acceleration, and hence, the acceleration phase prior to the dynamic rupture does not contribute significantly to the seismic wave radiation. Since the duration of the acceleration phase is quite long, quantifying the resulting aseismic deformation would allow us to assess whether the nucleation phase can be detected from near-field observations, an issue that we explore in the next section.

6. Magnitude and Duration of Precursory Signals

To assess whether the nucleation can be detected by near-field observations, we calculate the shear-strain rates $\dot{\varepsilon}$ induced by slip on the fault at a distance R from the eventual hypocenter of the simulated earthquakes following the widely used procedure of *Okada* [1992]. For simplicity, the calculations are done for an elastic whole space with uniform isotropic elastic properties. We focus our analysis on the scenarios with the wall rock near the SDZ and CDZ shown in Figure 4g.

Since the numerical fault model is 2-D (i.e., the fault is an infinite strip), we assume that the rupture area of the $M \sim 2$ repeating earthquakes is a 100 m by 100 m square fault patch and make a correction for the slip (and slip rate) difference between an infinite strip of width 100 m and a square of width 100 m. The relationship between the average slip $\overline{U}$ and uniform stress drop $\Delta\tau$ on a fault embedded into an elastic whole space is given by $\overline{U} = (\Lambda/C)(\Delta\tau/\mu')$, where Λ is the representative fault dimension and C is a nondimensional geometrical factor [*Scholz*, 2002]. The ratio of the average slip for a square fault of a width Λ to that for an infinite strip (in-plane shear) of the same width can be shown [*Parsons et al.*, 1988] as $\overline{U}_{\text{square}}/\overline{U}_{\text{in-plane}} = C_{\text{in-plane}}/C_{\text{square}} = 1.70/2.55 = 0.667$. Hence, the slip (and slip rate) on the square fault is smaller than that on the infinite strip, as expected. We then multiply slip rates during the simulated nucleation (Figures 4a and 4b) by this correction factor, $C_{\text{in-plane}}/C_{\text{square}}$. The corrected slip rates are assumed for the square fault patch and used for computing the corresponding strain rates in the Earth.

The square fault patch is discretized into many elongated, rectangular subfaults, each of which has the horizontal length of 0.0275 m and the vertical width of 100 m (Figure S3). A strain rate map at middepth is then calculated using the corrected slip rate distributions on the square fault. For each nucleation scenario, we use elastic constants estimated from the SAFOD geophysical log [*Zoback et al.*, 2011] (Table 1). Examples of a shear-strain rate map at different time snapshots are shown in Figure S4. We report the magnitude of shear-strain rates at off-fault distances R of 10, 100, and 1000 m (Figure S4).

Figure 4h shows that the magnitude of shear-strain rates $\dot{\varepsilon}$ at these observation points generally increases with time during the nucleation phase. Close ($R = 10$ m) to the fault, $\dot{\varepsilon}$ shows a decrease and then increase as the quasi-static rupture front migrates toward the center of the rate-weakening patch (Figure S4). Preseismic strain changes for a material with the properties of the wall rock near the CDZ are larger than those of the SDZ, even though h^*_{RR} for the CDZ is slightly smaller (Table 1). This can be explained by the difference in rate-and-state parameter a/b in the rate-weakening patch (Table 1). Since a/b for the CDZ is larger, the actively slipping zone during the nucleation is larger than that of the SDZ (Figures 4a and 4c), consistent with the theoretical result of *Ampuero and Rubin* [2008] in that nucleation sizes are generally larger for increasing a/b with the same $b - a$. Consequently, the larger nucleation zone for the CDZ results in larger preseismic strain changes (Figure 4h).

A few hours prior to the main shock, $\dot{\varepsilon}$ at $R = 100$ m is 2×10^{-12} s^{-1} for a material with the properties of the wall rock near the SDZ (Figure 4d). Hence, a strain of 7×10^{-9} would be measured in an hour period. Assuming that noise spectrum and detection threshold for subsurface strain measurements [*Agnew*, 1986; *Smith and Gomberg*, 2009] are applicable to measurements in a deep borehole, strains of $\gtrsim 10^{-9}$ would be detectable at an hour period, suggesting that the increase in strain rate is 7 times larger than the detectable level. On the other hand, the corresponding strain at $R = 1$ km is 10^{-11}, which is 2 orders of magnitude below the delectable level (Figure 4d). A similar inference can be drawn for a material with the properties of the wall rock near the CDZ (Figure 4d). Our results suggest that precursory aseismic slip of the Hawaii repeating earthquakes would be large enough to be detected by strainmeters situated within a few hundred meters from the hypocenter. This means that an array of strainmeters [e.g., *Blum et al.*, 2010] placed along the *existing* SAFOD borehole at ~2.7 km depth may enable the detection of such precursory slip.

7. Discussion and Conclusions

Using the model of earthquake nucleation validated with laboratory observations and combined with SAFOD drill core data, we have simulated the nucleation process of anticipated $M \sim 2$ repeating earthquakes on the San Andreas Fault. Despite up to 3 orders of magnitude difference in the physical and friction parameters and stress conditions, the behavior of the modeled nucleation qualitatively resembles that of laboratory earthquakes, with the nucleation consisting of two phases: initial slow rupture propagation and faster acceleration, both of which are likely aseismic processes, followed by dynamic rupture propagation that radiates seismic waves.

Our results indicate that the precursory deformation of the $M \sim 2$ earthquakes could be detected on the basis of near-field strain measurements hours before the occurrence of the earthquakes. However, the nucleation processes and the amount of preseismic strain changes would greatly depend on the in situ rate-and-state friction parameters (Figure 4). To robustly assess the detectability of the nucleation phase, one would need to systematically examine a wider range of nucleation scenarios, with more comprehensive measurements of friction parameters of drill core samples. In addition, the nucleation processes are simulated using 2-D models, and the corresponding preseismic strain changes for a 3-D source are calculated using corrected slip rate distributions, with some degree of approximation. In more realistic, yet computationally expensive 3-D models, an actively slipping zone during the nucleation tends to localize into a circular or elliptical region [e.g., *Kaneko et al.*, 2010; *Noda et al.*, 2013]. Hence, our estimates of preseismic strain changes (assuming a square source region) may have been slightly overestimated.

Our model implicitly assumes that the final dimension of earthquake rupture, or the size of an earthquake, is independent of the nucleation length as long as the critical length is less than the earthquake size. For example, critical nucleation lengths estimated from the physical and friction parameters of SAFOD samples appear to be of the order of tens of meters, which are smaller than the size of a typical $M \sim 2$ earthquake. Hence, our present study did not address whether the nucleation process of a larger earthquake can be captured by the near-field observations, which is an issue of societal importance. An important consequence of the above assumption is that a nucleation zone is not necessarily larger for a larger earthquake. Accelerating slow deformation associated with the nucleation phase of an earthquake has not yet been confidently detected anywhere; therefore, observing such precursor, even for the $M \sim 2$ repeating earthquakes, would open up a possibility for monitoring the nucleation process of a destructive large ($M > 6$) earthquakes.

The nucleation phase of earthquakes in mines has been studied by several investigators and is relevant to the findings in this study. For example, *Yabe et al.* [2015] inferred the nucleation process of a M 2 earthquake from the accelerating foreshock activities starting 7 days before the main shock. Given that physical conditions and near-field deformation in mines can be accurately monitored, it may be feasible to constrain the amplitude of precursory deformation signals expected from the nucleation process of earthquakes in mines using our modeling approach.

The present work utilizes advanced numerical models validated by laboratory observations and constrained by SAFOD fault zone drilling data to make testable predictions for the nucleation of anticipated repeating earthquakes at seismogenic depths. Such an integrated approach — the combination of numerical modeling, fault zone drilling data, and laboratory experiments — would contribute to the detection and understanding of largely unknown nucleation processes of crustal earthquakes at seismogenic depths.

Acknowledgments
We thank Jeff McGuire, Andrew Barbour, Andrea Llenos, Mauri McSaveney, and Grant Caldwell for their helpful discussions. We also thank two anonymous reviewers for their comments that helped us improve the manuscript. Y.K. was supported by a combination of the Marsden Fund administered by the Royal Society of New Zealand and by public funding from the Government of New Zealand. B.M.C. was funded by the ERC Starting Grant GLASS (259256). S.B.N. was partly funded by ERC Starting Grant NOFEAR (614705). Computer code used in this study is cited, and numerical data that support the conclusions are available from the corresponding author to anyone upon request.

References

Agnew, D. C. (1986), Strainmeters and tiltmeters, *Rev. Geophys.*, *24*(3), 579–624.
Ampuero, J.-P., and A. M. Rubin (2008), Earthquake nucleation on rate-and-state faults: Aging and slip laws, *J. Geophys. Res.*, *113*, B01302, doi:10.1029/2007JB005082.
Beeler, N. M., T. E. Tullis, and J. D. Weeks (1994), The roles of time and displacement in the evolution effect in rock friction, *Geophys. Res. Lett.*, *21*, 1987–1990, doi:10.1029/94GL01599.
Beeler, N. M., D. L. Lockner, and S. H. Hickman (2001), A simple stick-slip and creep-slip model for repeating earthquakes and its implication for microearthquakes at Parkfield, *Bull. Seismol. Soc. Am.*, *91*(6), 1797–1804.
Bhattacharya, P., A. M. Rubin, E. Bayart, H. M. Savage, and C. Marone (2015), Critical evaluation of state evolution laws in rate and state friction: Fitting large velocity steps in simulated fault gouge with time-, slip-, and stress-dependent constitutive laws, *J. Geophys. Res. Solid Earth*, *120*, 6365–6385, doi:10.1002/2015JB012437.
Blanpied, M. L., C. J. Marone, and D. A. Lockner (1998), Quantitative measure of the variation in fault rheology due to fluid-rock interactions, *J. Geophys. Res.*, *103*, 9691–9712, doi:10.1029/98JB00162.
Blum, J., H. Igel, and M. Zumberge (2010), Observations of Rayleigh-wave phase velocity and coseismic deformation using an optical fiber, interferometric vertical strainmeter at the SAFOD borehole, California, *Bull. Seismol. Soc. Am.*, *100*(5A), 1879–1891.
Bouchon, M., H. Karabulut, M. Aktar, S. Özalaybey, J. Schmittbuhl, and M.-P. Bouin (2011), Extended nucleation of the 1999 M_w 7.6 Izmit earthquake, *Science*, *331*(6019), 877–880, doi:10.1126/science.1197341.
Bouchon, M., V. Durand, D. Marsan, H. Karabulut, and J. Schmittbuhl (2013), The long precursory phase of most large interplate earthquakes, *Nat. Geosci.*, *6*(4), 299–302.
Campillo, M., and I. R. Ionescu (1997), Initiation of antiplane shear instability under slip dependent friction, *J. Geophys. Res.*, *102*(B9), 20,363–20,371.
Carpenter, B. M., D. M. Saffer, and C. Marone (2012), Frictional properties and sliding stability of the San Andreas fault from deep drill core, *Geology*, *40*(8), 759–762, doi:10.1130/G33007.1.
Carpenter, B. M., D. M. Saffer, and C. Marone (2015), Frictional properties of the active San Andreas Fault at SAFOD: Implications for fault strength and slip behavior, *J. Geophys. Res. Solid Earth*, *120*, 5273–5289, doi:10.1002/2015JB011963.
Chen, K. H., R. Bürgmann, R. M. Nadeau, T. Chen, and N. Lapusta (2010), Postseismic variations in seismic moment and recurrence interval of repeating earthquakes, *Earth Planet. Sci. Lett.*, *299*, 118–125, doi:10.1016/j.epsl.2010.1008.1027.
Chen, T., and N. Lapusta (2009), Scaling of small repeating earthquakes explained by interaction of seismic and aseismic slip in a rate and state fault model, *J. Geophys. Res.*, *114*, B01311, doi:10.1029/2008JB005749.
Collettini, C., A. Niemeijer, C. Viti, S. A. F. Smith, and C. Marone (2011), Fault structure, frictional properties and mixed-mode fault slip behavior, *Earth Planet. Sci. Lett.*, *311*(3), 316–327, doi:10.1016/j.epsl.2011.09.020.
Dieterich, J. H. (1979), Modeling of rock friction: 1. Experimental results and constitutive equations, *J. Geophys. Res.*, *84*, 2161–2168, doi:10.1029/JB084iB05p02161.
Dieterich, J. H. (1992), Earthquake nucleation on faults with rate- and state-dependent strength, *Tectonophysics*, *211*, 115–134, doi:10.1016/0040-1951(92)90055-B.
Dieterich, J. H., and B. H. Kilgore (1996), Implications of fault constitutive properties for earthquake prediction, *Proc. Natl. Acad. Sci. U.S.A.*, *93*(9), 3787–3794.
Dodge, D. A., G. C. Beroza, and W. L. Ellsworth (1996), Detailed observations of California foreshock sequences: Implications for the earthquake initiation process, *J. Geophys. Res.*, *101*(B10), 22,371–22,392.
Fang, Z., J. H. Dieterich, and G. Xu (2010), Effect of initial conditions and loading path on earthquake nucleation, *J. Geophys. Res.*, *115*, B06313, doi:10.1029/2009JB006558.
Gao, H., D. A. Schmidt, and R. J. Weldon (2012), Scaling relationships of source parameters for slow slip events, *Bull. Seismol. Soc. Am.*, *102*(1), 352–360.
Hickman, S., and M. Zoback (2004), Stress orientations and magnitudes in the SAFOD pilot hole, *Geophys. Res. Lett.*, *31*, L15S12, doi:10.1029/2004GL020043.
Hickman, S., M. Zoback, and W. Ellsworth (2004), Introduction to special section: Preparing for the San Andreas Fault Observatory at Depth, *Geophys. Res. Lett.*, *31*, L12S01, doi:10.1029/2004GL020688.
Hori, T., N. Kato, K. Hirahara, T. Baba, and Y. Kaneda (2004), A numerical simulation of earthquake cycles along the Nankai trough, Southwest Japan: Lateral variation in frictional property due to slab geometry controls the nucleation position, *Earth Planet. Sci. Lett.*, *228*, 215–226.
Ikari, M. J., A. R. Niemeijer, and C. Marone (2011a), The role of fault zone fabric and lithification state on frictional strength, constitutive behavior, and deformation microstructure, *J. Geophys. Res.*, *116*, B08404, doi:10.1029/2011JB008264.
Ikari, M. J., C. Marone, and D. M. Saffer (2011b), On the relation between fault strength and frictional stability, *Geology*, *39*(1), 83–86, doi:10.1130/G31416.1.
Kanamori, H., and D. L. Anderson (1975), Theoretical basis of some empirical relations in seismology, *Bull. Seis. Soc. Amer.*, *65*, 1073–1095.
Kaneko, Y., and J.-P. Ampuero (2011), A mechanism for preseismic steady rupture fronts observed in laboratory experiments, *Geophys. Res. Lett.*, *38*, L21307, doi:10.1029/2011GL049953.
Kaneko, Y., and N. Lapusta (2008), Variability of earthquake nucleation in continuum models of rate-and-state faults and implications for aftershock rates, *J. Geophys. Res.*, *113*, B12312, doi:10.1029/2007JB005154.
Kaneko, Y., J.-P. Avouac, and N. Lapusta (2010), Towards inferring earthquake patterns from geodetic observations of interseismic coupling, *Nat. Geosci.*, *3*, 363–369, doi:10.1038/NGEO843.
Kaneko, Y., S. B. Nielsen, and B. M. Carpenter (2016), The onset of laboratory earthquakes explained by nucleating rupture on a rate-and-state fault, *J. Geophys. Res. Solid Earth*, *121*, 6071–6091, doi:10.1002/2016JB013143.
Kato, A., K. Obara, T. Igarashi, H. Tsuruoka, S. Nakagawa, and N. Hirata (2012), Propagation of slow slip leading up to the 2011 M_w 9.0 Tohoku-Oki earthquake, *Science*, *335*(6069), 705–708, doi:10.1126/science.1215141.
Kato, N., and T. Hirasawa (1996), Effects of strain rate and strength nonuniformity on the slip nucleation process: A numerical experiment, *Tectonophysics*, *265*(3), 299–311.
Kato, N., K. Yamamoto, H. Yamamoto, and T. Hirasawa (1992), Strain-rate effect on frictional strength and the slip nucleation process, *Tectonophysics*, *211*(1), 269–282.
Lapusta, N., and Y. Liu (2009), Three-dimensional boundary integral modeling of spontaneous earthquake sequences and aseismic slip, *J. Geophys. Res.*, *114*, B09303, doi:10.1029/2008JB005934.
Lapusta, N., and J. R. Rice (2003), Nucleation and early seismic propagation of small and large events in a crustal earthquake model, *J. Geophys. Res.*, *108*(2205), doi:10.1029/2001JB000793.

Latour, S., A. Schubnel, S. Nielsen, R. Madariaga, and S. Vinciguerra (2013), Characterization of nucleation during laboratory earthquakes, *Geophys. Res. Lett.*, *40*, 5064–5069, doi:10.1002/grl.50974.
Liu, Y., and N. Lapusta (2008), Transition of mode II cracks from sub-Rayleigh to intersonic speeds in the presence of favorable heterogeneity, *J. Mech. Phys. Solids*, *56*, 25–50.
Marone, C., and D. M. Saffer (2015), The mechanics of frictional healing and slip instability during the seismic cycle, in *Treatise on Geophysics*, 2nd ed., pp. 111–138, The Pennsylvania State Univ., University Park. doi:10.1016/B978-0-444-53802-4.00092-0.
McGuire, J. J., M. Boettcher, and T. H. Jordan (2005), Foreshock sequences and earthquake predictability on East Pacific rise transform faults, *Nature*, *434*, 457–461, doi:10.1038/nature03377.
McLaskey, G. C., and B. D. Kilgore (2013), Foreshocks during the nucleation of stick-slip instability, *J. Geophys. Res. Solid Earth*, *118*, 2982–2997, doi:10.1002/jgrb.50232.
Mitchell, E. K., Y. Fialko, and K. M. Brown (2016), Velocity-weakening behavior of Westerly granite at temperature up to 600°C, *J. Geophys. Res. Solid Earth*, *121*, 6932–6946, doi:10.1002/2016JB013081.
Moore, D. E., and M. J. Rymer (2012), Correlation of clayey gouge in a surface exposure of serpentinite in the San Andreas Fault with gouge from the San Andreas Fault Observatory at Depth (SAFOD), *J. Struct. Geol.*, *38*, 51–60, doi:10.1016/j.jsg.2011.11.014.
Moore, D. E., D. A. Lockner, and S. Hickman (2016), Hydrothermal frictional strengths of rock and mineral samples relevant to the creeping section of the San Andreas Fault, *J. Struct. Geol.*, *89*, 153–167, doi:10.1016/j.jsg.2016.06.005.
Nielsen, S., J. Taddeucci, and S. Vinciguerra (2010), Experimental observation of stick-slip instability fronts, *Geophys. J. Int.*, *180*, 697–702, doi:10.1111/j.1365-246X.2009.0444.x.
Noda, H., M. Nakatani, and T. Hori (2013), Large nucleation before large earthquakes is sometimes skipped due to cascade-up—Implications from a rate and state simulation of faults with hierarchical asperities, *J. Geophys. Res. Solid Earth*, *118*, 2924–2952, doi:10.1002/jgrb.50211.
Ohnaka, M. (1996), Nonuniformity of the constitutive law parameters for shear rupture and quasistatic nucleation to dynamic rupture: A physical model of earthquake generation processes, *Proc. Natl. Acad. Sci. U.S.A.*, *93*(9), 3795–3802.
Ohnaka, M., and Y. Kuwahara (1990), Characteristic features of local breakdown near a crack-tip in the transition zone from nucleation to unstable rupture during stick-slip shear failure, *Tectonophysics*, *175*(1), 197–220.
Okada, Y. (1992), Internal deformation due to shear and tensile faults in a half-space, *Bull. Seismol. Soc. Am.*, *82*, 1018–1040.
Okubo, P. G., and J. H. Dieterich (1984), Effects of physical fault properties on frictional instabilities produced on simulated faults, *J. Geophys. Res.*, *89*(B7), 5817–5827.
Parsons, I. D., J. F. Hall, and G. A. Lyzenga (1988), Relationships between the average offset and the stress drop for two- and three-dimensional faults, *Bull. Seismol. Soc. Am.*, *78*(2), 931–945.
Paul, J., and C. P. Rajendran (2015), Short-term pre-2004 seismic subsidence near South Andaman: Is this a precursor slow slip prior to a megathrust earthquake?*Phys. Earth Planet. Inter.*, *248*, 30–34, doi:10.1016/j.pepi.2015.08.006.
Rathbun, A. P., and C. Marone (2013), Symmetry and the critical slip distance in rate and state friction laws, *J. Geophys. Res. Solid Earth*, *118*, 3728–3741, doi:10.1002/jgrb.50224.
Reinen, L. A., J. D. Weeks, and T. E. Tullis (1991), The frictional behavior of serpentinite: Implications for aseismic creep on shallow crustal faults, *Geophys. Res. Lett.*, *18*(10), 1921–1924, doi:10.1029/91GL02367.
Rice, J. R. (1993), Spatio-temporal complexity of slip on a fault, *J. Geophys. Res.*, *98*(B6), 9885–9907, doi:10.1029/93JB00191.
Rubin, A. M. (2008), Episodic slow slip events and rate-and-state friction, *J. Geophys. Res.*, *113*, B11414, doi:10.1029/2008JB005642.
Ruina, A. L. (1983), Slip instability and state variable friction laws, *J. Geophys. Res.*, *88*, 10,359–10,370, doi:10.1029/JB088iB12p10359.
Schmitt, S. V., P. Segall, and T. Matsuzawa (2011), Shear heating-induced thermal pressurization during earthquake nucleation, *J. Geophys. Res.*, *116*, B06308, doi:10.1029/2010JB008035.
Scholz, C. H. (2002), *The Mechanics of Earthquakes and Faulting*, 2nd ed., 496 pp., Cambidge Univ. Press, New York.
Schurr, B., et al. (2014), Gradual unlocking of plate boundary controlled initiation of the 2014 Iquique earthquake, *Nature*, *512*(7514), 299–302.
Shibazaki, B., and M. Matsu'ura (1998), Transition process from nucleation to high-speed rupture propagation: Scaling from stick-slip experiments to natural earthquakes, *Geophys. J. Int.*, *132*(1), 14–30, doi:10.1046/j.1365-246x.1998.00409.x.
Smith, E. F., and J. Gomberg (2009), A search in strainmeter data for slow slip associated with triggered and ambient tremor near Parkfield, California, *J. Geophys. Res.*, *114*, B00A14, doi:10.1029/2008JB006040.
Tape, C., M. West, V. Silwal, and N. Ruppert (2013), Earthquake nucleation and triggering on an optimally oriented fault, *Earth Planet. Sci. Lett.*, *363*, 231–241.
Tullis, T. E. (1996), Rock friction and its implications for earthquake prediction examined via models of Parkfield earthquakes, *Proc. Natl. Acad. Sci. U.S.A.*, *93*(9), 3803–3810.
Viesca, R. C. (2016), Stable and unstable development of an interfacial sliding instability, *Phys. Rev. E*, *93*(6), doi:10.1103/PhysRevE.93.060202.
Wei, M., Y. Kaneko, Y. Liu, and J. J. McGuire (2013), Episodic fault creep events in California controlled by shallow frictional heterogeneity, *Nat. Geosci.*, *6*, 566–570, doi:10.1038/ngeo1835.
Yabe, Y., M. Nakatani, M. Naoi, J. Philipp, C. Janssen, T. Watanabe, T. Katsura, H. Kawakata, G. Dresen, and H. Ogasawara (2015), Nucleation process of an $M2$ earthquake in a deep gold mine in South Africa inferred from on-fault foreshock activity, *J. Geophys. Res. Solid Earth*, *120*, 5574–5594, doi:10.1002/2014JB011680.
Zoback, M., et al. (2011), Scientific drilling into the San Andreas Fault Zone—An overview of SAFOD's first five years, *Sci. Drill.*, *11*(1), 14–28.

Supporting Information for article "Nucleation process of magnitude 2 repeating earthquakes on the San Andreas Fault predicted by rate-and-state fault models with SAFOD drill core data"

Yoshihiro Kaneko[1], Brett M. Carpenter[2,3], Stefan B. Nielsen[4]

S1. Description of model parameters

In laboratory-scale simulations considered in *Kaneko et al.* [2016], the model parameters replicate the experimental set-up [*Latour et al.*, 2013] (Table 1). At the same time, the rate-and-state parameter $a - b$, characteristic slip distance D_c, and the background loading rate $\dot{\tau}$ were not well constrained in the laboratory experiments. Hence we vary these parameters within a realistic range. Table 1 shows a set of parameters that best reproduces the characteristics of shear-rupture nucleation observed in the laboratory experiments with different normal stresses. In laboratory-scale simulations shown in Figure 1f, we set $\dot{\tau} = 0.36$ MPa/s, compatible with the estimated loading rate of the order of 0.4 MPa/s in the laboratory experiments of *Nielsen et al.* [2010]. Note that our modeling results are independent of the reference friction coefficient f_0 and reference slip rate V_0 as long as f_0 is greater than the change in frictional resistance resulting from fault slip and healing.

To ensure well-resolved simulations, proper numerical parameters are carefully selected. The spatial cell size Δx needs to be small enough to resolve both the process zone size during quasi-static nucleation [e.g., *Ampuero and Rubin*, 2008] and cohesive-zone size during dynamic rupture propagation [e.g., *Kaneko et al.*, 2008]. A grid spacing Δx is chosen such that the nucleation length is resolved by at least 300 node points. We find that such grid spacing leads to well-resolved simulations in this study. As described in [*Lapusta and Liu*, 2009], time t is discretized into variable time steps, with the minimum value of $\Delta t_{\min}$ given by $\Delta x/(3V_s) = 0.03$ and 10 microseconds (μs) for laboratory-scale and crustal-scale simulations, respectively, where V_s is the shear wave speed of the medium. Such a small value of $\Delta t_{\min}$ is necessary as slip in one time step must be smaller than the characteristic slip D_c of the friction law. The total number of time steps in each simulation shown in Figure 4 is ∼3 million.

[1]GNS Science, Avalon, Lower Hutt, New Zealand
[2]School of Geology and Geophysics, University of Oklahoma, Norman, OK, 73019
[3]Istituto Nazionale di Geofisica e Vulcanologia, Rome, Italy
[4]Department of Earth Sciences, University of Durham, United Kingdom

0094-8276/17/$5.00

References

Ampuero, J.-P., and A. M. Rubin (2008), Earthquake nucleation on rate-and-state faults: aging and slip laws, *J. Geophys. Res.*, *113*, B01302, doi:10.1029/2007JB005082.

Kaneko, Y., N. Lapusta, and J.-P. Ampuero (2008), Spectral element modeling of spontaneous earthquake rupture on rate and state faults: Effect of velocity-strengthening friction at shallow depths, *J. Geophys. Res.*, *113*, B09317, doi:10.1029/2007JB005553.

Kaneko, Y., S. B. Nielsen, and B. M. Carpenter (2016), The onset of laboratory earthquakes explained by nucleating rupture on a rate-and-state fault, *J. Geophys. Res.*, *121*, 6071–6091, doi:10.1002/2016JB013143.

Lapusta, N., and Y. Liu (2009), Three-dimensional boundary integral modeling of spontaneous earthquake sequences and aseismic slip, *J. Geophys. Res.*, *114*(B9), doi:10.1029/2008JB005934.

Latour, S., A. Schubnel, S. Nielsen, R. Madariaga, and S. Vinciguerra (2013), Characterization of nucleation during laboratory earthquakes, *Geophys. Res. Lett.*, *40*(19), 5064–5069, doi:10.1002/grl.50974.

Nielsen, S., J. Taddeucci, and S. Vinciguerra (2010), Experimental observation of stick-slip instability fronts, *Geophys. J. Int.*, *180*, 697–702, doi:10.1111/j.1365-246X.2009.0444.x.

Corresponding author: Y. Kaneko, GNS Science, 1 Fairway Drive, Avalon, Lower Hutt, New Zealand. (y.kaneko@gns.cri.nz)

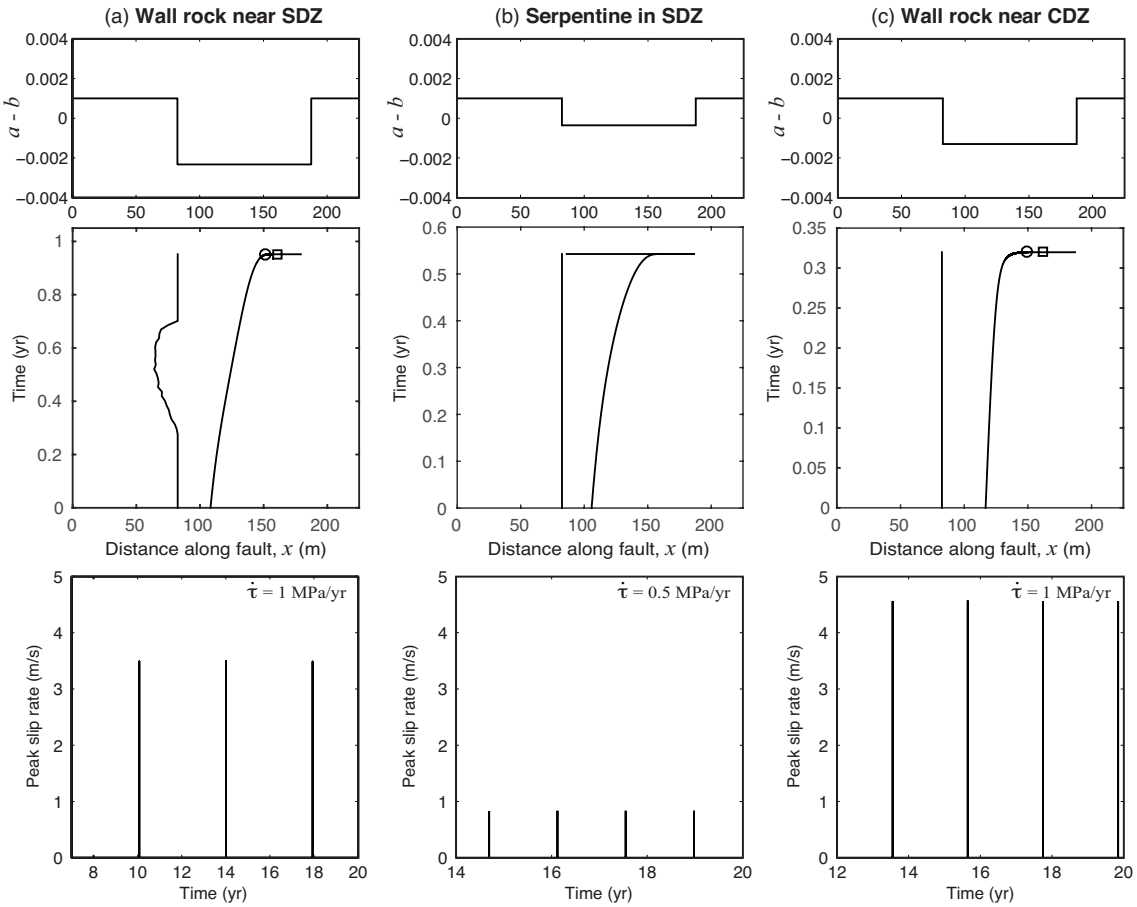

Figure S1. Simulated nucleation processes of SAFOD repeating earthquakes using materials with the properties of (a) wall rock near the SDZ, (b) serpentine in the SDZ and (c) Wall rock near the CDZ. Distribution of friction parameter $a - b$ (top panel), rupture front positions during the nucleation process (middle panel), and the evolution of the peak slip rate over the several earthquake cycles (bottom panel) are shown for each case. Rupture fronts are defined as the locations of two peak shear stresses: one within the left rate-strengthening patch and the other within the rate-weakening patch. We use measured values of friction parameters (Table 1) for the central rate-weakening patch. In the rate-strengthening segments, b is chosen such that $a - b = 0.001$. Other physical parameters are constrained by geophysical log data at the SAFOD depths. Transitions from quasi-static to acceleration phase (open circle) and from acceleration to dynamic propagation (open square) during the nucleation process are indicated. Assumed background loading rates are also indicated.

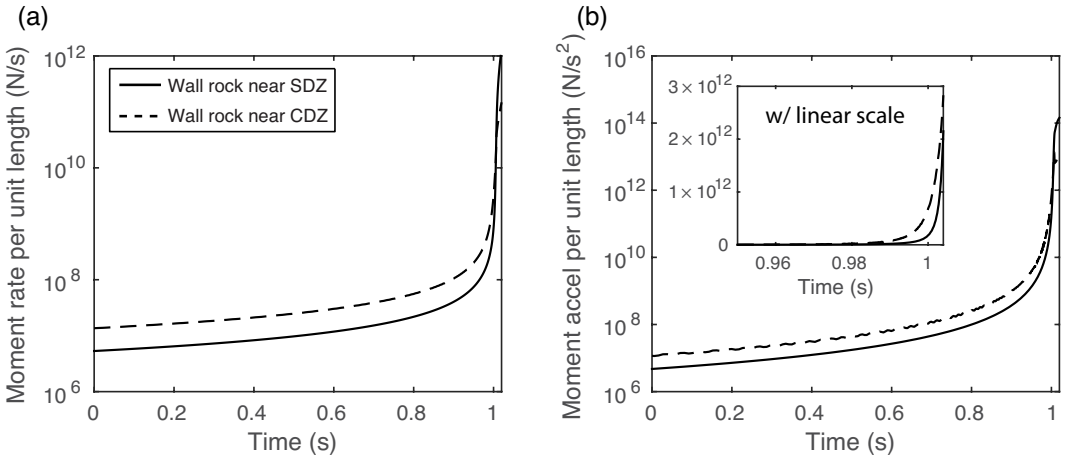

Figure S2. (a) Moment rate and (b) moment acceleration, as a function of time, for the materials with the properties of wall rocks near the SDZ and the CDZ. Time is chosen such that $t = 1$ s roughly corresponds to the onset of the dynamic rupture propagation. The inset shows a zoom-in view of moment acceleration on a linear scale.

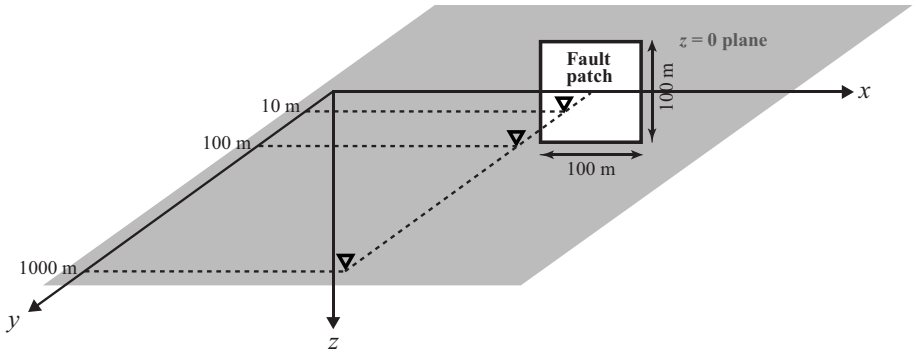

Figure S3. Fault geometry and domain in which the strain rates are computed for the simulated nucleation of SAFOD earthquakes. We assume that a fault patch that ruptures coseismically during the Hawaii repeating earthquakes is a 100 m by 100 m square. The square fault is composed of many elongated, rectangular sub-faults, each of which is characterised by a uniform slip rate at a given instant in time. The open triangles correspond to receiver locations at which the evolution of strain rates is reported in Figure 4h.

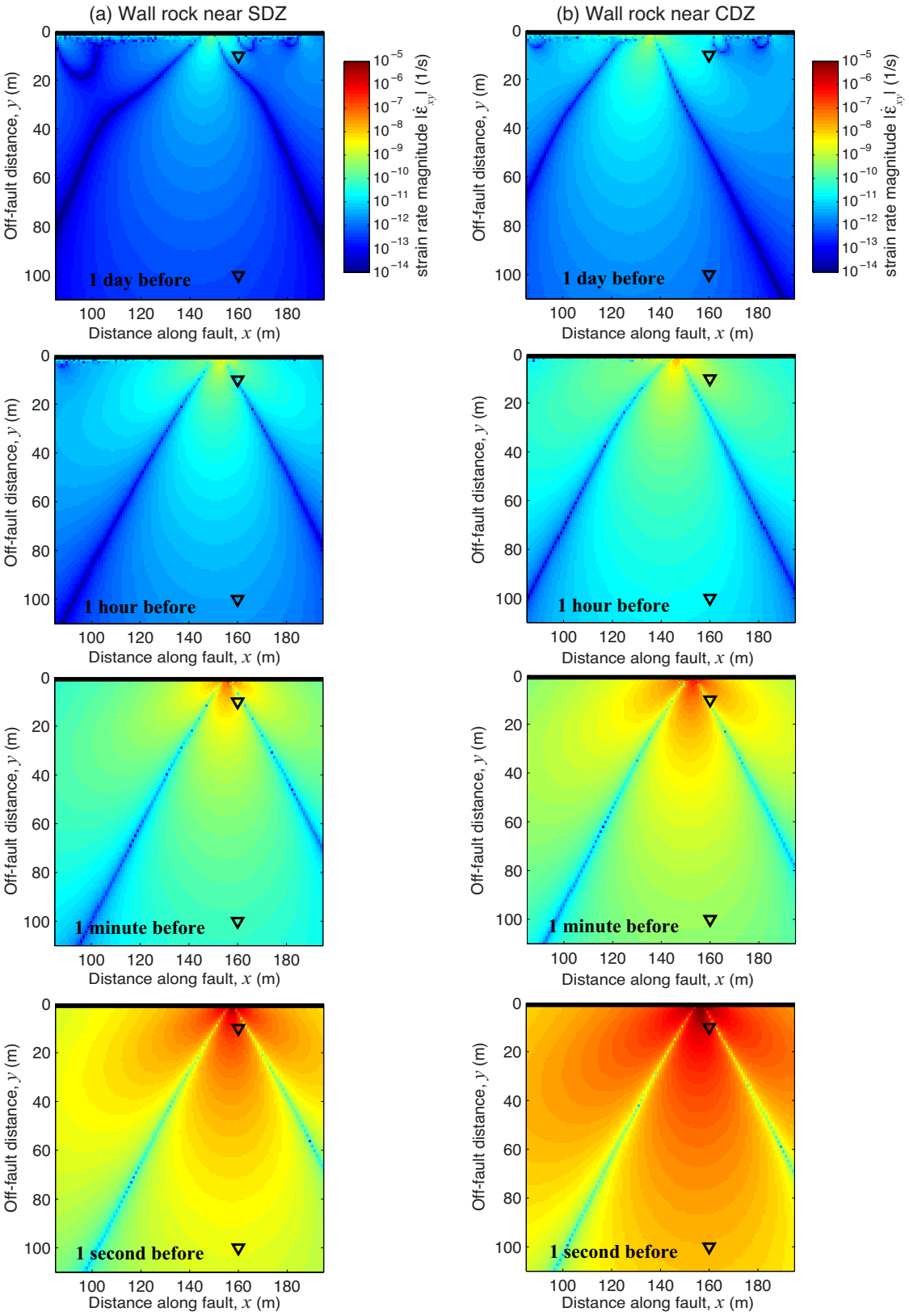

Figure S4. Snapshots of the magnitude of shear-strain rates associated with the simulated nucleation process of SAFOD repeating earthquakes for materials with the properties of wall rocks near (a) the SDZ and (b) the CDZ. The fault is located along the $y = 0$ line. The open triangles are receivers located at $(x, y) = (160, 10)$ m and $(160, 100)$ m. In both cases, the eventual dynamic rupture propagation begins at $(x, y) = (160, 0)$ m, signifying the hypocenter of the earthquakes.